Fermi National Accelerator Laboratory

FERMILAB-Pub-88/44
[VPI-IHEP 88/2]

Search for Neutral Metastable Penetrating Particles Produced in the SLAC Beam Dump*

(SLAC Experiment E-137)

J. D. Bjorken
Fermi National Accelerator Laboratory
P.O. Box 500, Batavia, Illinois 60510

S. Ecklund and W. R. Nelson
Stanford Linear Accelerator Center
Stanford, California 94305

A. Abashian, C. Church*, B. Lu, L. W. Mo,
T. A. Nunamaker†, and P. Rassmann††
Physics Department,
Virginia Polytechnic Institute and State University
Blacksburg, Virginia 24061

April 1988

*Submitted to Phys. Rev.
*Permanent address: Datec, Inc., 7061 Manchester Avenue, Hanover Park, Illinois 60103
†Also, Nanometrics, Inc., 451 South Boulevard, Oak Park, Illinois 60302
††Present address: Siemens U8 333, Frauenauracher Str. 85, 8520 Erlangen, Tennenlohe, West Germany

Search for Neutral Metastable Penetrating Particles Produced in the SLAC Beam Dump

(SLAC Experiment E-137)

J.D. BJORKEN
Fermi National Accelerator Laboratory, Batavia Il. 60510

S. ECKLUND AND W.R. NELSON
Stanford Linear Accelerator Center, Stanford, Calif. 94305

A. ABASHIAN, C. CHURCH*, B. LU, L.W. MO,
T.A. NUNAMAKER†, AND P. RASSMANN††
Physics Department, Virginia Polytechnic Institute
and State University, Blacksburg, Va. 24061

Abstract

A search was made for neutral objects which might be produced by 20 GeV electrons incident on the SLAC beam dump, penetrate the downstream natural shielding, and decay upstream of an electromagnetic shower calorimeter. With about 30 coulombs of electrons dumped, no candidate events were found above an energy of ~ 2 GeV. The 95% confidence level limit on the product of mass and lifetime of light axion-like bosons decaying primarily into two photons is determined to be greater than 1.4 keV-sec. Limits on photino parameters are also given.

---

* Permanent address: Datec, Inc., 7061 Manchester Avenue, Hanover Park, Il. 60103.

† Also, Nanometrics Inc., 451 South Blvd., Oak Park, Il. 60302.

†† Present Address: Siemens U8 333, Frauenauracher Str. 85, 8520 Erlangen, Tennenlohe, West Germany

I. INTRODUCTION

In this article, we describe an experimental search for neutral objects which might be produced in the electromagnetic showers initiated by 20 GeV electrons in the SLAC beam dump. The objects of search would have to penetrate 200 m of earth shielding and decay in a 200 m region downstream of the shield. If the decay products contained electrons, positrons, and/or photons, they could be detected by an electromagnetic shower counter located downstream of the decay region.

There are several classes of conjectured low-mass, neutral particles with little coupling to matter which are of special interest as objects of such an experimental search. Among candidate objects are neutral neutrino-like leptons, the photinos of super-symmetric theories, and axions. However, it must be kept in mind that the most relevant object in such a speculative search experiment as this may well be "none of the above". For example, the predecessor[1] of the present experiment, SLAC experiment E56 (M. Schwartz, spokesman) had as a primary motivation the search for ν_τ-like neutrinos. But it turned out to be of interest with respect to axion searches. This experiment, SLAC experiment E137, was primarily motivated as an axion search, but also has some sensitivity as a photino search.

There are features of this beam-dump experiment quite unique to SLAC. There is the high intensity of the primary beam, with a yield of approximately one coulomb of 20 GeV electrons delivered per (very good) day. The 1.6 μsec pulse length (180 pulses/sec) allows good cosmic-ray rejection. But most importantly the electrons, positrons, and photons which are produced in the dump (aluminum plates immersed in a large tank of water) have transverse momenta no larger than 20 MeV, much lower than in hadronic showers. This

collimation, together with production mechanisms even more collimated, implies that beams of the sundry hypothetical particles will be well collimated. This in turn allows a long decay region without significant loss of acceptance. The E-137 apparatus is located about 380 m downstream of the dump, with 200 m of available decay path in front of the detector. This geometry is typical of hadron dump experiments with more than an order of magnitude higher energy.

Typical collimated production mechanisms are shown in Fig. 1. They include coherent photoproduction of bosons which could then decay into $\gamma\gamma$ or e^+e^-, bremsstrahlung of bosons from electrons followed by decay into e^+e^-, or annihilation of positrons upon atomic electrons, either resonantly (again followed by e^+e^- decay) or nonresonantly into a pair of particles such as photinos. (The photino purportedly decays into γ + gravitino).

With such a lengthy longitudinal geometry and the resultant reliance on collimation, the sensitivity of the experiment is best for low masses, well below 100 MeV. The best experimental sensitivity occurs for candidates with small production cross-section and long lifetime. For example, a 10 MeV particle with lifetime ~ 10^{-8} sec and production cross-section ~ 10^{-44} cm^2 would be detectable; longer presumed lifetimes would imply a proportionately larger cross-section bound. Detailed limits will be discussed later in the context of more specifically defined objects of search.

II. OBJECTS OF SEARCH

A. Generic Axions

Neutral spinless mesons of nearly zero mass arise[2] in many theories constraining spontaneously broken symmetry: these are the pseudo-Nambu-Goldstone-bosons, or "generic axions". Such particles couple to the divergence of the current whose charge generates the symmetry which is spontaneously broken. Because the mass is small, the corresponding charge must be (almost) conserved; in the limit of exact conservation the mass vanishes.

In general, there are many cases to consider, e.g. whether or not the conjectured charge-operator contains quark fields and/or whether it contains lepton fields. There may be axions whose current contains only unknown degrees of freedom.

While no model other than the original[3,4] Peccei-Quinn-Weinberg-Wilczek (PQWW) axion,* provides parameters relevant to this search, it is still just as important to search for "generic axions" as to search for unanticipated new quarks, leptons, or heavy gauge bosons.

The axion species most relevant to this experiment are those which do not couple significantly to quarks. What is important is that the particle does couple to $\gamma\gamma$ and/or e^+e^-. The phenomenology then depends only upon the assumed widths $\Gamma(x \to \gamma\gamma)$ and $\Gamma(x \to e^+e^-)$, and upon the assumed mass.

*Our nomenclature is that the PQWW axion is the axion, and all axions (other than the "invisible axions") are "generic".

The relevant production mechanisms are shown in Fig. 1. They include Primakoff production, bremsstrahlung from the incident electron, and resonant or radiative annihilation of positrons on atomic electrons. The cross-sections and convolutions over primary flux are discussed in Appendix A. For bremsstrahlung and Primakoff mechanisms, and for low-mass axions, the yield per radiation length is proportional to Γ_x/M_x^3, as might be anticipated from dimensional considerations. The decay probability is proportional to $\Gamma_x/\gamma_x \sim M_x\Gamma_x/\langle E_x \rangle$. The net yield is therefore proportional to Γ_x^2/M_x^2, and for long lifetimes and low mass one will find a bound on the product $M_x\tau_x$. For short lifetimes, one demands the particle penetrate the earth shield before decaying: $\gamma_x c\tau_x \gtrsim L$. That limit is therefore controlled by τ_x/M_x. For such a limit, this experiment, with its thick shield of 200 m, is not competitive with its predecessor, SLAC experiment E56, or other recent short-dump experiments.[5]

B. Photinos

Some phenomenological supersymmetry schemes have posited a light photino decaying into photon and gravitino. This neutral particle has spin 1/2; the gravitino is the spin 3/2 partner of the graviton. In this experiment, photino pairs might be produced in e^+e^- annihilation (on atomic electrons) via scalar-electron (selectron) exchange. The yield thus depends not only on photino mass and lifetime but also quite sensitively to the selectron mass. The photino lifetime in turn depends upon the scale $\Lambda = \sqrt{d}$ of symmetry breaking, conjectured to perhaps be in the range of 100 GeV to 10 TeV. The experiment is sensitive only to a narrow range of photino masses, but within that range the sensitivity exceeds that attained in more general searches carried out in e^+e^- colliders.[6]

III. THE EXPERIMENT

A sketch of the experimental layout is shown in Fig. 2. The SLAC primary electron beam was transported through End-Station A, site of the classic deep-inelastic electron scattering experiments. Then the beam continued through a vacuum pipe to reach Beam Dump East, located in the berm at the downstream end of the SLAC research area, where all the beam power was absorbed in an assembly of aluminum plates interlaced with cooling water. After Beam Dump East, a hill of 179 m in thickness served as additional absorber for all known particles other than neutrinos. The detector, an electromagnetic shower counter with excellent angular resolution, was located across a valley from this hill, with 204 m of decay path between the exit point of the beam from the hill and the detector.

A. Beam Setup

The beam transport to End Station A acted as a double focusing spectrometer with an energy-defining slit located at the intermediate focus. From End Station A to Beam Dump East, the beam was made parallel. There were no magnetic elements in this portion of the beam transport system. The intensity of the beam was measured by two 33" diameter toroids on a pulse-to-pulse basis. The typical momentum spread of the beam was $\Delta p/p = 1\%$.

In End Station A, a remotely controllable aluminum target of various thicknesses could be inserted into the beam to generate beam-associated "skyshine" background. Charged pions produced in this target emerged into the air space above the top of the hill which was viewed by the detector. These pions could interact with the air, producing at the detector mainly muons (along with a few photons) coming from decaying pion secondaries. These "skyshine" particles were very useful for timing the electronics and setting the experimental gate, as well as for checking out and monitoring

detector performance. During the data-taking with the beam dump, the target was of course removed, and the primary electron beam was transported, without changing steering, to Beam Dump East.

In order to reduce skyshine background considerable concrete shielding was added around the beam transport through End Station A. A lead wall at the upstream end of End Station A was also useful in reducing skyshine from sources immediately upstream of End Station A.

The direction and focusing of the electron beam between End Station A and Beam Dump East was checked with remotely controlled roller screens. The screens were coated with ZnS material and marked with a fiducial grid. The luminescence of the screen when bombarded with electrons allowed fine adjustment of steering and focussing. After adjustment and during data taking, the screens were moved to a position with empty holes, such that the beam transversed the hole without intercepting any material.

B. The Detector

The detector consisted of an 8-layer, 8 radiation length shower calorimeter. Each layer consisted of a hodoscope of 1.5 m x 0.5 m x 1 cm plastic scintillation counters, one radiation length of iron or aluminum converter, and one multiwire proportional chamber. For the first phase of the experiment (~10 coulombs of 20 GeV electrons dumped), each plane was a 2 x 3 mosaic of the 1 m x 1 m proportional chambers[7] used in the Fermilab experiment of Heisterberg et. al.[8] which measured ν_μe elastic scattering; aluminum radiator was used. For the final phase of the experiment (~20 Coulombs of 20 GeV electrons dumped) new 3 m x 3 m proportional chambers of similar design were installed, and the aluminum radiator was replaced by steel.

Clearly good angular resolution (<<50 mrad) was essential, and this capability was obtained from the multiwire proportional chambers. As shown in Fig. 3, the two cathode planes of the chambers consist of delay lines milled from copper-clad G10, one for horizontal readout, the other for vertical. Each delay line was tapped at several points (5 for the 1 m x 1 m chambers, and 24 for the 3 m x 3 m chambers) and each cathode signal was fed into a charge-coupled-device (CCD) operating at 50 MHz. In order to reduce the attenuation, the delay lines on the 3 m x 3 m chambers were cut into 23 pieces. 22 of them had readout on one end only, and one was read out from both ends. The CCD, acting as a fast analogue shift register, subdivided an incoming pulse into 20 nsec segments and stored the charge of each segment into consecutive CCD "buckets". When a trigger from the scintillation hodoscope occured, the CCD clock rate was reduced to 20 MHz until the charges stored in the 36 "buckets" of each CCD could be digitized in sequence by one analogue-to-digital converter (ADC). This provided essentially analogue information on the cathode pulse size and shape, with a spatial resolution of ~ 3 mm for the 3 m x 3 m chambers and ~ 8 mm for the original 1 m x 1 m chambers.

The charge coupled devices were manufactured by Fairchild, with model number CCD321A. They had approximately 8-bit dynamic range, 320 buckets long. As mentioned above, only the first 36 buckets were used, operating at 50 MHz clock rate, and whenever a trigger occurred, the clock rate had to be decreased to 20 MHz while the stored charges were shifted to the end of the CCD. This mode of operation reduced the charge transfer loss to a negligible level.

C. Experimental Trigger

Two triggering schemes were used in parallel. The first emphasized energy and required that the total pulse height (per scintillator plane) in three of any four adjacent planes be above a preassigned threshold. The threshold shower energy for this trigger was 400 MeV. The second trigger, which emphasized directionality, was highly efficient even for horizontal muons, and required at least four of eight 1.5m x 0.5m x 1cm scintillation counters in a given horizontal row (i.e. having the same transverse location in the apparatus) to fire in coincidence. Here the signals were amplified, with a gain of 10, before each discriminator, and the discriminator thresholds were set well below the minimum ionizing level. These two triggers were linked with a logical "or" to provide the master trigger for the experiment. The schematics of the trigger electronics is shown in Figure 4.

Once a trigger occurred, data from the CCD's, ADC's, scalars, and latches were read into the on-line computer via a standard CAMAC dataway, and then logged onto magnetic tape. The computer used for the experiment was a Data General 16-bit, Eclipse S/230 which was also used to monitor the performance of experimental apparatus in standard manner.

D. Calibration of Equipment

The high voltages on the 96 plastic scintillation counters, 1.5 m x 0.5 m x 1 cm in size, were set by a procedure to be described below. Each counter was placed behind a ~4 radiation length aluminum plate. An electron beam was sent through the counter at exactly the same relative geometric position. The high voltage on the counter was adjusted until the pulse height spectrum became identical in both magnitude and shape as compared to a standard spectrum. The SLAC test beam was most versatile for this purpose.

The beam intensity could go as low as 1 electron/pulse and the energy could be varied from 1 GeV to 14 GeV. With this procedure, all 96 scintillation counters were set to the same gain.

In February, 1984, energy calibrations were performed in the SLAC test beam on the scintillation hodoscopes. A stack of eight counters with steel radiators, identical to those used in the experiment, was put into the electron test beam. Pulse height from each individual counter was recorded. The calibrations were done at energies from 1 to 14 GeV. Data were also collected with beam hitting different positions of the counter.

The 48 1 m x 1 m chambers were used for several years at Fermilab in doing the $\nu_\mu e$ elastic scattering experiment. These chambers had been calibrated at Cornell and Fermilab using electrons of energies from 2 to 30 GeV. Therefore, the calibrations were known and we did not calibrate them again at SLAC. The eight 3 m x 3 m chambers were quite bulky. To set them up in the test beam would have been quite a job. As a result, we did not calibrate these chambers. The high voltage was set by their responses to high energy horizontal muons. Because these chambers were only used for track measurements in this experiment, this practice was adequate. In all cases, the energy measurements were done by the scintillation counters.

E. Experimental Running

The experiment was proposed and approved in 1980. The first run, with 9.5 Coulombs of electrons dumped, occured in January of 1982. The final run, with 20.4 Coulombs of electrons dumped, occurred in November and December 1982. In February, 1984, the scintillation hodoscopes was calibrated in the SLAC test beam.

The running conditions turned out to be quite clean. With a 1/4" aluminum target inserted into the beam at End Station A, the skyshine trigger rate was approximately 3×10^6/Coulomb, dominated by low energy muons. The energy spectrum of these beam associated triggers is shown in Figure 5. Essentially nothing is found above an energy of 3 GeV. Figure 6 shows the time distribution of the triggers when the aluminum target was in the beam. The beam associated triggers were clearly seen above the general cosmic ray backgrounds. This time distribution was used to check the beam gate for the experiment.

With the target removed, the triggers were dominated by cosmic rays with a typical rate of $\sim 10^3$/Coulomb. The energy spectrum is considerably harder, as shown in Figure 7. Of course, the angular distribution is much broader, leading to easy rejection of almost all these triggers. Examination of the time distribution of the low energy component of the spectrum does reveal a beam-associated signal. If the energy spectrum of that beam-associated signal is the same as for "target-in" data, there should be in the data sample less than 0.2 beam-associated triggers per Coulomb with energy above 3 GeV.

IV. DATA ANALYSIS

After the final run in late 1982, the data was analyzed with the aid of computer-generated visual displays. Firstly, the data was processed with very few cuts. The only requirements were that the data should be within the 2 μsec gate around the beam time and the estimated shower energy should be greater than 1 GeV. This simple procedure immediately removed ~75% of the data. For example, for the final 20 Coulomb run, out of ~23,000 trigger written on tape, only ~6,000 of them survived the cut. These events were then examined in detail on a high resolution graphics terminal. There were 12 horizontal columns of scintillation counters, each 8 layers deep. First the pulse height distributions in these 12 columns of scintillators were displayed on the graphics terminal, together with other relevant information such as total energy, timing, etc. One could readily categorize the majority of these events as muons or cosmic ray showers. Another useful display was the x- and y-views of all the chambers. The pulse height information from all the CCD's was displayed simultaneously, so that one could immediately see the tracks in each view as well as the shower development along the track. A typical event as seen by the multiwire proportional chambers in shown in Figure 8. After this computer-aided scan, where events which were observed to be grossly nondirectional were rejected, 189 events remained. These were measured, and after cuts requiring vertical and horizontal angles less than 300 mrad, only 24 events remained. Those within ±140 mrad are shown in Figure 9. One sees that only one event lies within a reasonable fiducial region of horizontal angle less than ±100 mrad and vertical angle less than 30 mrad (the approximate horizon of the shielding berm as seen by the detector). Just from the multiwire proportional chamber data this surviving event may be regarded as pointing toward the beam dump. But it has too low an energy; 2 GeV was the optimistic threshold cut. Combining the chamber and scintillator information, this event can be understood as a muon radiating a photon in the

front portion of the detector and penetrating the entire eight layers of detector. We thus end up with no convincing candidate events.

For the earlier dump run with ~10 Coulombs of 20 GeV electrons, the detector was smaller, 2 m x 3 m, as described above. Using the same method of analysis for 5600 triggers written on tape, also no candidate events were found.

A second line of analysis was also used which avoided possible subjectivity associated with the visual scanning. (However, in a search experiment such as this, and with the complex topology of the typical cosmic ray triggers, we believe there is no substitute for making the full scan.) In this alternative analysis, we required that the observed energy exceeded 3 GeV, that the signal be in time with the beam, and that at least 2/3 of the energy be within a single row of scintillators, as would be expected for almost all horizontal showers. Only 36 events passed these criteria, and the event sample overlapped the preceding sample of 189 obtained from the visual scan, again leading to no candidate events.

V. DISCUSSION OF RESULTS

A. Axions

We assume that the candidate generic axion is photoproduced via the Primakoff effect, decays predominantly into two photons or an e^+e^- pair and is of low mass. Under these circumstances, the experimental yield depends only upon mass, M_X, and lifetime, τ_X. Figure 10 shows the experimental result on the lower limit of the product $M_X\tau_X$ as a function of axion mass M_X, for the case of axions decaying into two photons. If the axion has significant coupling to e^+e^- and mass above 1 MeV, it will preferentially decay into that mode. Figure 11 shows the experimental limit on $M_X\tau_X$ vs M_X for the case of axions decaying into e^+e^- pairs, assuming "generic" coupling strength F_X to $\gamma\gamma$ and e^+e^-. Figure 12 and Figure 13 show the axion decay coupling constant F_X as a function of the axion mass. Details of the calculations and theoretical assumptions are given in Appendix 1.

In calculating the experimental limit on $M_X\tau_X$, a threshold energy cut of 2 GeV was used. The expected energy spectrum of axions is proportional to the track-length distribution of photons in the beam dump. This was computed using the EGS shower program,[9] which is shown in Figure 14. One can see that ~30% of the expected axion flux above 1 GeV actually lies above 3 GeV. Thus our quoted limit (which scales with the square root of the flux) is not inordinately sensitive to the cut in energy.

There are also other axion production processes which are equally important. They include axion bremsstrahlung from the electrons or positrons, and the annihilation of positrons with atomic electrons into axion plus a photon. Their limits on $M_X\tau_X$ and F_X are shown in Figures 15 through 18. Calculational details are again given in Appendix 1.

The classical Peccei-Quinn-Weinberg-Wilczek (PQWW) axion[3,4] has by now been convincingly ruled out experimentally. The sensitivity of this experiment to a PQWW axion is marginal, and is shown in Figure 19. Were the PQWW axion to exist, experiment E-137 might have seen it. But E-137 never could have ruled out the whole mass range of 100 to 400 KeV which was of interest a few years ago.[10]

However, it still remains important to search for generic axion-like entities (i.e. pseudo Nambu-Goldstone bosons) associated with perhaps some totally unanticipated spontaneous symmetry-breaking scheme remote from present experience. The present result most improves previous bounds on parameters if the axion-like entity is not coupled to currents containing known lepton or quark degrees of freedom.

B. Photinos

As discussed in Section II, photino pairs might be produced in e^+e^- annihilation on atomic electrons via selectron exchange.[11] To estimate the yield, the positron flux in the dump was computed via the EGS code. When convoluted with the production cross-section and decay lifetime,[12] the yield of decay photons in the detector was calculated as function of the presumed selectron mass and symmetry breaking scale $\sqrt{d}$. The limit from this experiment is shown in Figure 20. To our knowledge the region excluded by this experiment has not been fully covered by previous measurements.[6]

VI. ACKNOWLEDGEMENTS

We thank W. K. H. Panofsky and the SLAC staff for generous support and assistance. Special thanks go to Finn Halbo for superb engineering support and to the accelerator operations crew, who delivered beam of record intensity under difficult operating conditions. This research was supported in part by the Department of Energy, the National Science Foundation (Grant No. PHY-8218233), and a fellowship to one of us (L.W. Mo) by the J.S. Guggenheim Foundation.

APPENDIX A

Calculations of Event Rate

To determine the event rates in the SLAC beam dump experiment, we have to first calculate the spectra of photons, electrons, and positrons produced in the beam dump by the primary electron beam from the accelerator. This was done with the code of the SLAC EGS program.[9] Typical examples of these spectra are shown in Figure 14.

Once the γ, e^-, e^+ spectra in the beam dump were known, then the mechanisms for productions of axions were considered. They included the Primakoff production of axions by photons, "bremsstrahlung" of axions by electrons or positrons in the scattering process, and annihilations of high energy positrons in the beam dump by atomic electrons. The Feynman diagrams of these processes are shown in Figure 1. After the production calculations, the axions were followed through the decay region. The probability of the axion decaying in flight into $\gamma\gamma$ or e^+e^- was computed and folded with the geometric acceptance of the detector to give the final answers for the rates measured by the detector.

The flux of photons, electrons and positrons in the beam dump are all functions of both energy and angle. This is also true for the production and decay of the axion, as well as the geometric acceptance of the detector. Therefore it is appropriate to describe in more detail how the calculations were carried out.

The 3 m x 3 m detector, located 383 m downstream from Beam Dump East, was considered as mosaic of 144 small pieces. The number of photons per energy bin (or e^-,e^+) aimed at each one of these 144 pieces of detector was computed using the EGS code. A low energy threshold cut of either 2 or 3 GeV was applied to the

spectrum in each one of these "small" detectors. Then the energy spectrum was divided into consecutive ΔE bins of 1 GeV. The number of γ's (or e^-,e^+) in each ΔE bin of this "small" detector was then considered as "mono-energetic". It was used together with the production cross sections to compute the axion spectra aimed at each "small" detector into ΔE bins. Axions in each one of these ΔE bins were also considered monoenergetic. The axions were then followed through the shielding and into the decay space in front of the detector (204 m). Then the acceptance along the flight path was folded in for each of the 144 "small" detectors. The rates were expressed in terms of two unknown parameters, the axion mass M_x and its decay coupling constant F_x.

The formulae used for various production processes are summarized below:

(A) Primakoff Production

The cross section for photoproduction of axions via the Primakoff mechanism is given by

$$\frac{d\sigma}{d\Omega} = 8\alpha \frac{\Gamma}{M_x^3} |F(t)|^2 \frac{\theta^2}{(\theta^2+\delta^2)^2} \tag{A1}$$

where Γ is the decay width assumed rather arbitrarily[13] to be

$$\Gamma(x \to \gamma\gamma) = \frac{\alpha^2}{64\pi^3}\left(\frac{M_x^3}{F_x^2}\right), \tag{A2}$$

Likewise we assume a generic coupling M_x/F_x to electrons, which gives

$$\Gamma(x \to e^+e^-) = \frac{m_e^2(M_x^2 - 4m_e^2)^{1/2}}{8\pi F_x^2} \quad . \tag{A3}$$

and

$$\delta = \frac{1}{2}\left(\frac{M_x}{E_\gamma}\right)^2 \tag{A4}$$

t = 4-momentum transfer squared to the target (t<0),

F(t) = form factor of target.

Since we are concerned only with low momentum transfers, it suffices to consider only the atomic form factors and the elastic scattering form factor of the nuclei. The atomic form factor is parametrized as

$$|F(t)|^2 = Z^2\left(\frac{a^2|t|}{a^2|t|+1}\right) + Z\left(\frac{a'^2|t|}{a'^2|t|+1}\right)^2 \tag{A5}$$

where the parameters a and a' are given as[14]

$$a = \frac{122.8}{m_e} \quad \text{for hydrogen,}$$

$$= 111 \frac{Z^{-1/3}}{m_e} \quad \text{for oxygen,}$$

$$a' = \frac{282.4}{m_e} \quad \text{for hydrogen,} \tag{A6}$$

$$= 773 \frac{Z^{-2/3}}{m_e} \quad \text{for oxygen.}$$

For protons, the dipole form factor is used[15]

$$G_E = \frac{G_M}{\mu_p} = \frac{1}{(1 + \frac{|t|}{0.71})^2} \tag{A7}$$

where μ_p is the anomalous magnetic moment of proton. For the oxygen nucleus, this elastic form factor is given by[15]

$$F = Z \left(1 + \frac{a_o^2 t}{8}\right) e^{a_o^2 t/4} \tag{A8}$$

where $a_o = 8.97$.

(B) "Bremsstrahlung" Production of Axions in Electron Scattering:

For electron (or positron) scattering from nuclear targets, the axion can be radiated from the electron. The cross section is given[16] by

$$\frac{d^2\sigma}{d\Omega_x dE_x}(E_+,E_x,\theta) = \frac{\alpha^2\alpha_s}{\pi}\frac{x(1-x)}{D^2}E_+\left(\frac{x^2}{(1-x)} - \frac{2xM_x^2}{D} + \frac{2M_x^2}{D^2}\left[(1-x)M_x^2+x^2m_e^2\right]\right)\chi \tag{A9}$$

where

$$E_+ = \text{incoming electron energy},$$

$$E_x = \text{outgoing axion energy},$$

$$\alpha_s = \frac{1}{4\pi}\left(\frac{m_e}{F_x}\right)^2$$

$$x = \frac{E_x}{E_+} \ ,$$

$$D = M_x^2\ \frac{(1-x)}{x} + m_e^2x + xE_+^2\theta^2 \ ,$$

$$P_+ = \sqrt{E_+^2 - m_e^2} \ ,$$

$$P_x = \sqrt{E_x^2 - M_x^2} \ ,$$

$$\chi = \int_{t_{min}} |F(t)|^2 \cdot \frac{(t-t_{min})}{t^2}\,dt. \tag{A10}$$

(C) Production of Axions by the Annihilation Process $e^+e^- \rightarrow x^o\gamma$:

The cross section is given by

$$\frac{d\sigma}{d(\cos\theta^*)} = \frac{g^2\alpha}{2s}\left(\frac{M_x^2}{s-M_x^2}\right)\frac{1}{(1-\beta\cos\theta^*)(1+\beta\cos\theta^*)} \qquad \text{(A11)}$$

where

$$g = \frac{m_e}{F_x} \ ,$$

s = C.M. energy squared,

θ^* = polar angle of axion in the center of mass system.

β = speed of electron target in C.M. system. (A12)

Apparently, this cross section has an infrared divergence when the photon energy is low. A low energy cut of 3 MeV was applied to the photon in the center of mass system in the rate calculations.

(D) Production of Photino Pairs via $e^+e^- \to \tilde{\gamma}\tilde{\gamma}$

The cross section in the C.M. system is given by[11]

$$\frac{d\sigma}{d\Omega_{CM}} = \frac{\alpha^2 s}{8m_{\tilde{e}}^4} (1+\cos^2\theta_{\tilde{\gamma}})\beta^3 \qquad \text{(A13)}$$

where

$m_{\tilde{e}}$ = mass of the selectron,

$$\beta^3 = \left(1 - \frac{4m^2_{\tilde{\gamma}}}{s}\right)^{3/2}, \text{ (p-wave factor)} \qquad \text{(A14)}$$

The decay width of a photino into a real photon and a gravitino is given by

$$\Gamma(\tilde{\gamma} \to \gamma + \tilde{G}) = \left(\frac{\tilde{m}^5}{8\pi d^2}\right), \qquad \text{(A15)}$$

where $\tilde{m}$ is the photino mass, and the parameter d has the dimension of $(\text{mass})^2$ and measures the scale of the supersymmetry breaking.

Figure Captions

Fig. 1. Collimated production mechanism for neutral bosons: (a) Primakoff photoproduction, (b) bremsstrahlung from electrons, (c) resonant annihilation of positrons on atomic electrons, and (d) nonresonant production (by positrons on atomic electrons) of photino pairs via selectron exchange.

Fig. 2. Layout of SLAC experiment E-137.

Fig. 3. Schematic of the delay-line multiwire proportional chambers and the CCD electronics.

Fig. 4. Schematic of the trigger electronics.

Fig. 5. Energy spectrum of experimental triggers as determined from total scintillator pulse height for beam-associated skyshine with removable aluminum target in the beam.

Fig. 6. Time distribution of beam-associated triggers when aluminum target was in the beam.

Fig. 7. Energy spectrum of experimental triggers as determined from total scintillator pulse height for beam dump running with target removed.

Fig. 8. Typical event as seen by the 3 m x 3 m multiwire proportional chambers. On the left is the top view of the chambers. The ticks locate the taps on the delay line. The bold-faced region is that portion of the chamber read by the CCD's which is shown expanded on the right, where the observed pulse shape is exhibited. The peak values have been plotted on the layout at the left.

Fig. 9. Scatter plot of the angular distribution of candidate events. Only the bold-faced point has energy >3 GeV; the triangular point has energy >2 GeV, but unambiguously does not point toward the dump. The three points apparently emergent from below the horizon are actually cosmic rays entering the detector from the rear.

Fig. 10. Limits (95% confidence level) on hypothetical axion properties from experiment E-137. It is assumed the axion decays predominantly into $\gamma\gamma$.

Fig. 11. Limits on hypothetical axion properties from experiment E-137. It is assumed the axion decays predominantly into e^+e^-.

Fig. 12. Exclusion plot for axion mass and lifetime parameters, assuming Primakoff photoproduction and a standardized "generic" coupling F_x to two photons (cf Appendix I, Eqn. A2).

Fig. 13. Exclusion plot for axion mass and lifetime parameters, assuming Primakoff photoproduction and a standardized "generic" coupling M_x/F_x to electrons (cf Appendix I, Eqn. A3).

Fig. 14. Track-length distribution T(E) of photons, electrons and positrons, in the SLAC beam dump. The normalization is such that, for example the photoproduced axion yield dN/dE per incident is given by

$$\frac{dN}{dE} = T(E) \cdot \sum_{Z} \sigma(\gamma+Z \rightarrow x+Z) P_Z$$

where P_Z is the number density of atoms (per cm^{-3}) of atomic number Z.

Fig. 15. Exclusion plot for axion mass and lifetime parameters assuming bremsstrahlung from electrons and positrons and a standardized "generic" coupling F_x to $\gamma\gamma$ and e^+e^- (cf Appendix I, Eqns. A2 and A3).

Fig. 16. Exclusion plot as in Fig. 15 for F_x and m_x.

Fig. 17. Exclusion plot for axion mass and lifetime parameters assuming positron annihilation on atomic electrons via $e^+e^- \rightarrow x + \gamma$ and subsequent decay into e^+e^-.

Fig. 18. Exclusion plot as in Fig. 17 for F_x and m_x.

Fig. 19. Limits on axion properties assuming coupling only to $\gamma\gamma$; the predicted properties of the PQWW axion are also shown.

Fig. 20. Exclusion plot for photino mass as function of symmetry breaking scale $\sqrt{d}$ and assumed selectron mass, as discussed in the text and Appendix A.

REFERENCES

1. T.W. Donnelly, S.J. Freedman, R.S. Lytel, R.D. Peccei, and M. Schwartz, Phys. Rev. D18, 1607(1978).

2. Y. Declais, Proceedings of the 21st International Conference on High Energy Physics, July 1982, Paris, France, ed. P. Petiau and M. Porneuf.

3. R.D. Peccei and H.R. Quinn, Phys. Rev. Lett. 38, 1440(1977).

4. S. Weinberg, Phys. Rev. Lett. 40, 223(1978).
F. Wilczek, Phys. Rev. Lett. 40, 279(1978).

5. For a recent review, see M. Davier, Proceedings of the 23rd International Conference on High Energy Physics, July 1986, Berkeley, CA., ed. S. Loken, Vol. 1, p. 25.

6. For a summary of limits on photino parameters, see for example J.F. Grivaz, Proceedings of the 23rd International Conference on High Energy Physics, July 1986, Berkeley, CA., ed. S. Loken, Vol. 1, p. 614.

7. T.A. Nunamaker, R.H. Heisterberg, and L.W. Mo, Nucl. Instr. Meth. 175, 331(1980).

8. R.H. Heisterberg, L.W. Mo, and T.A. Nunamaker; K.A. Lefler and A. Skuja; A. Abashian; N.E. Booth; C.C. Chang, C.L., and C.H. Wang; Phys. Rev. Lett. 44, 635(1980).

9. W.R. Nelson, H. Hirayama, and D. Rogers, SLAC Report 265 (1986).

10. H. Faissner et. al., Phys. Lett. 103B, 234(1981).

11. P. Fayet, Phys. Rev. Lett. 86B, 272(1979); Phys. Lett. 117B, 460(1982); Proceedings of the 21st International Conference on High Energy Physics, July 1982, Paris, France, ed. P. Petiau and M. Perneuf; J. Ellis and J. Hagelin, Phys. Lett. 122B, 303(1983).

12. A. Halprin, C.M. Anderson, and H. Primakoff, Phys. Rev. 152, 1295(1966).

13. This corresponds to a calculation via the triangle anomaly, where the contributing fermions satisfy
$$\sum_i T_3{}^i Q_i^2 = 1.$$

14. K.J. Kim and Y.S. Tsai, Phys. Rev. D8, 3109(1973); Y.S. Tsai, Rev. Mod. Phys. 46, 815(1974).

15. R. Hofstadter, Ann. Rev. Nucl. Sci. 7, 231(1957).

16. Y.S. Tsai, Phys. Rev. D34, 1326(1986).

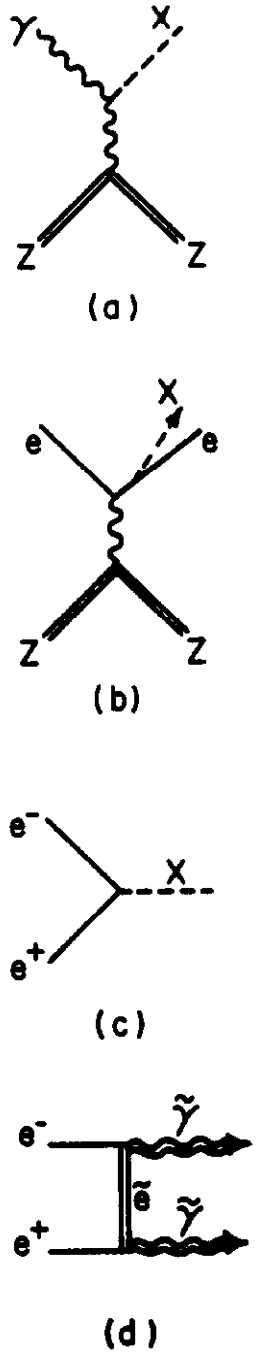

FIGURE 1

Collimated production mechanism for neutral bosons: (a) Primakoff photoproduction, (b) bremsstrahlung from electrons, (c) resonant annihilation of positrons on atomic electrons, and (d) nonresonant production (by positrons on atomic electrons) of photino pairs via selectron exchange.

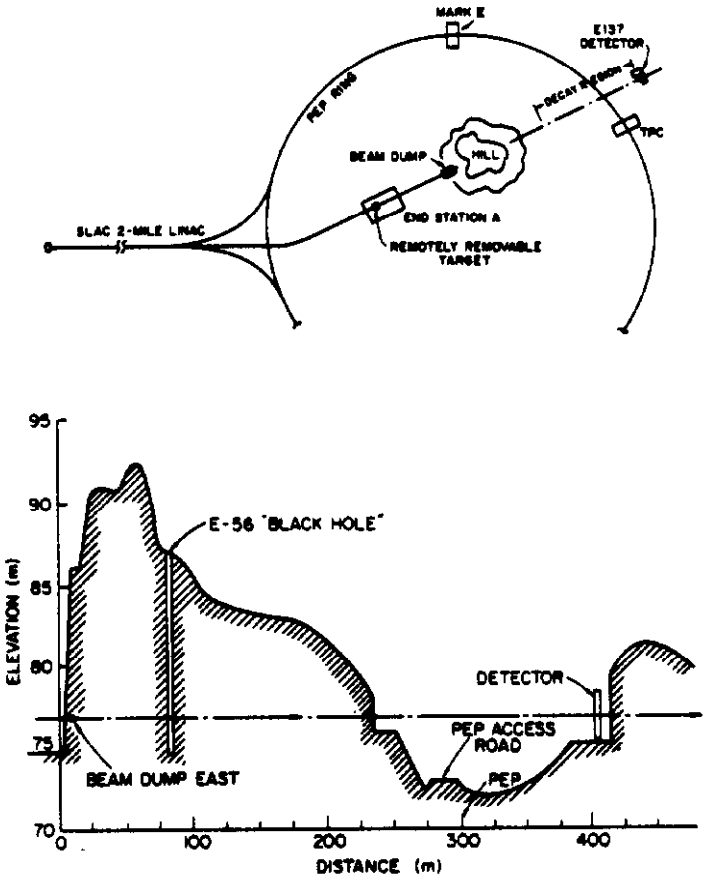

FIGURE 2

Layout of SLAC experiment E-137.

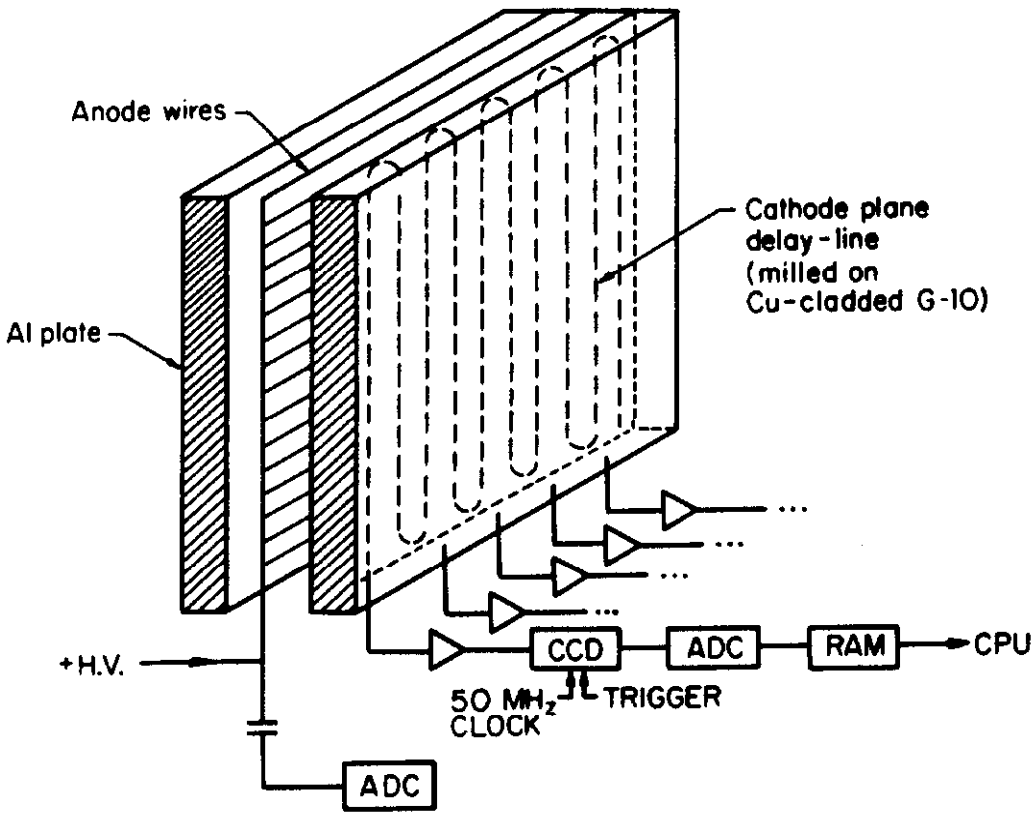

FIGURE 3

Schematic of the delay-line multiwire proportional chambers and the CCD electronics.

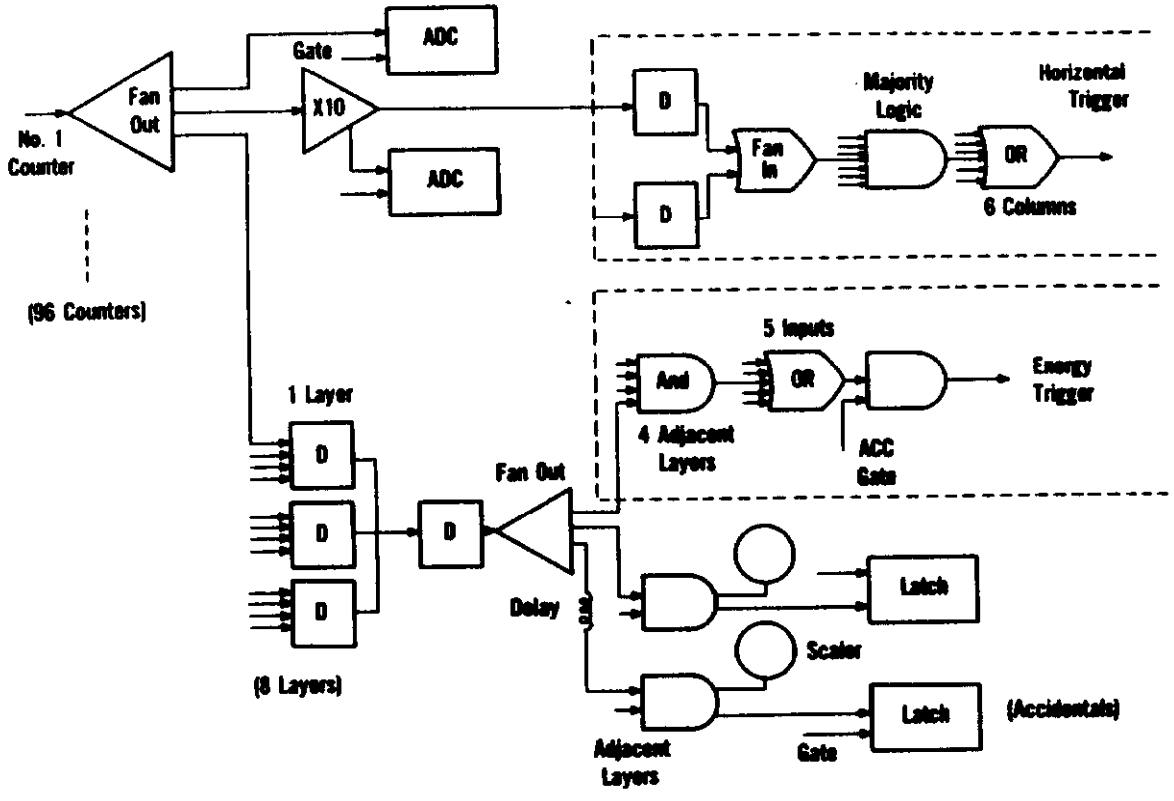

FIGURE 4

Schematic of the trigger electronics.

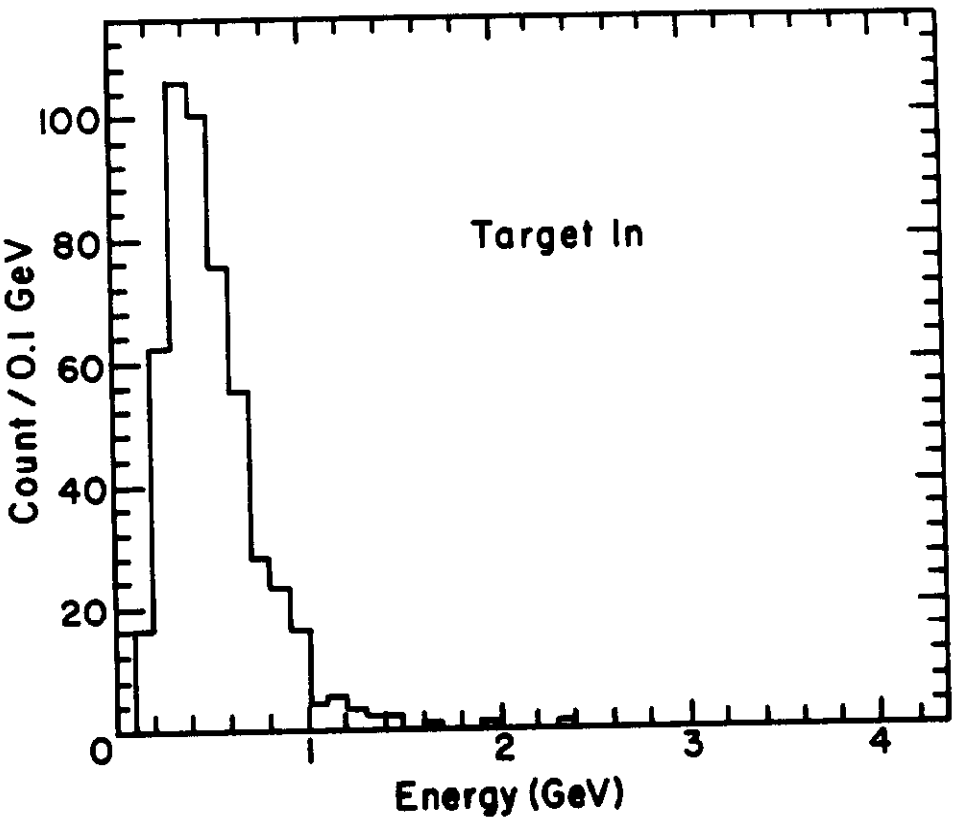

FIGURE 5

Energy spectrum of experimental triggers as determined from total scintillator pulse height for beam-associated skyshine with removable aluminum target in the beam.

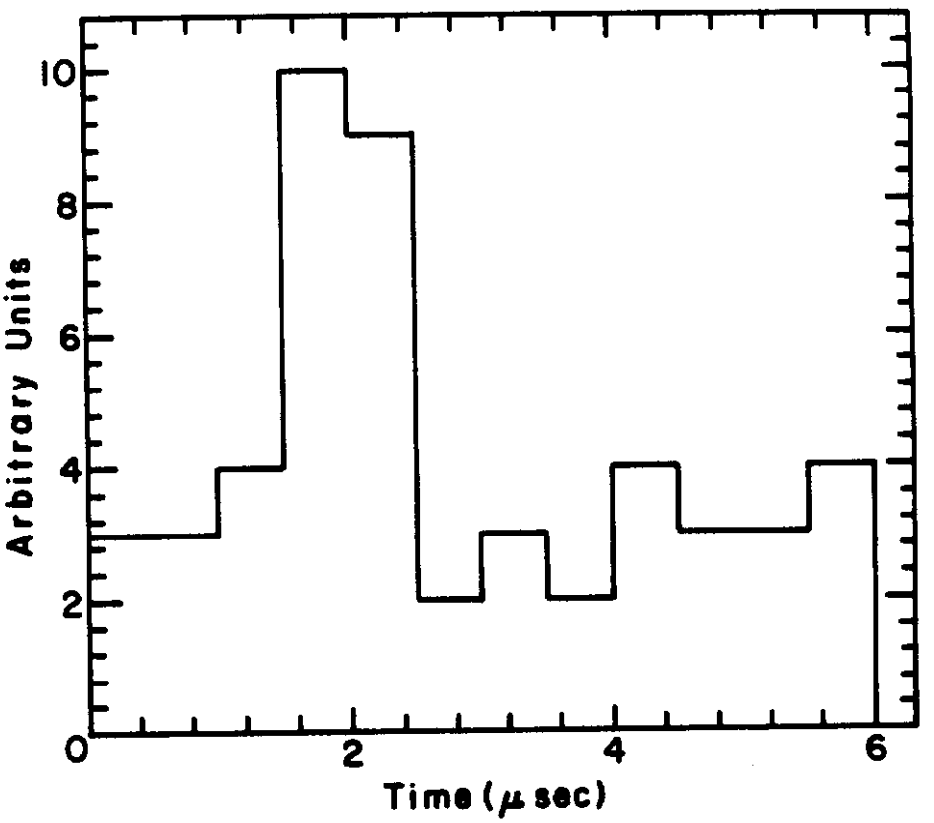

FIGURE 6

Time distribution of beam-associated triggers when aluminum target was in the beam.

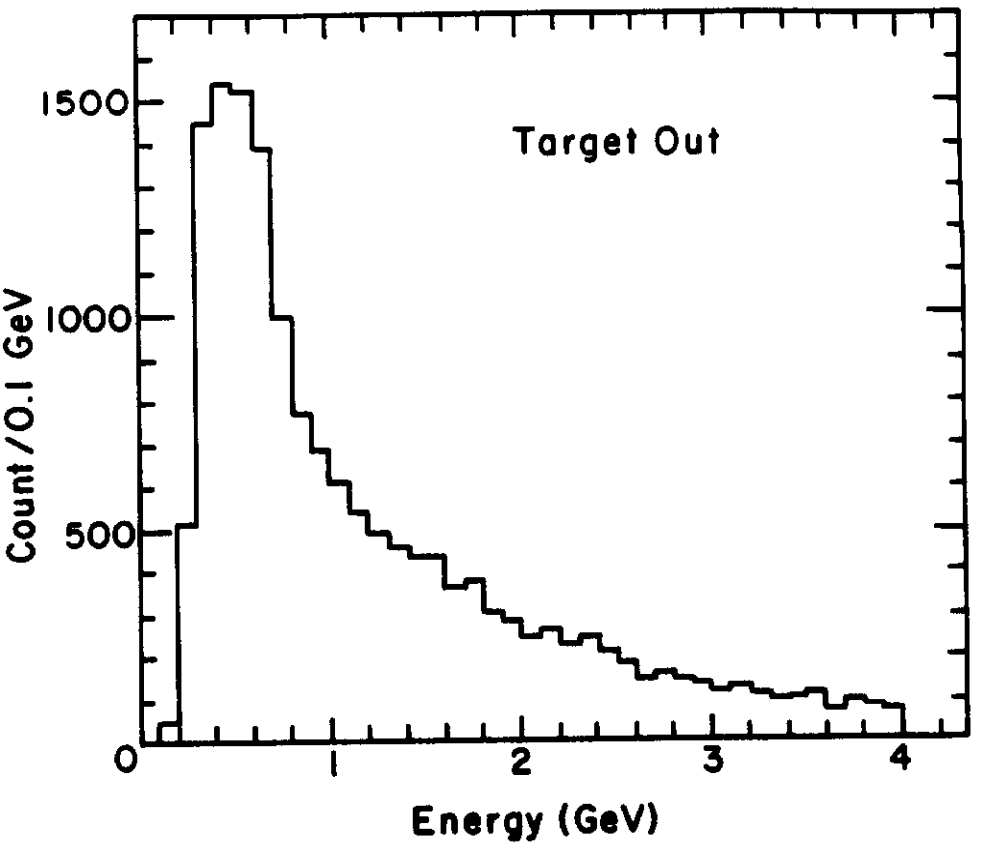

FIGURE 7

Energy spectrum of experimental triggers as determined from total scintillator pulse height for beam dump running with target removed.

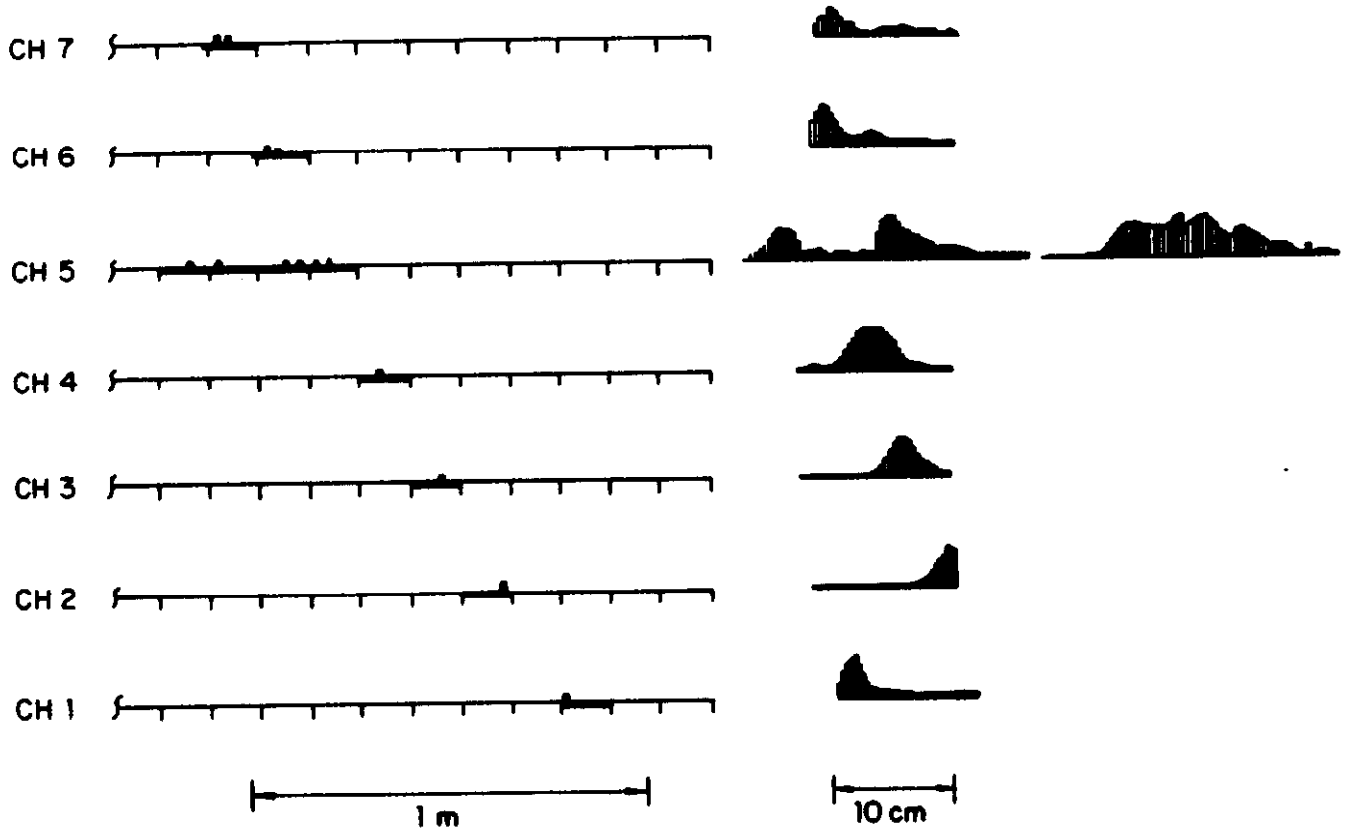

FIGURE 8

Typical event as seen by the 3 m x 3 m multiwire proportional chambers. On the left is the top view of the chambers. The ticks locate the taps on the delay line. The bold-faced region is that portion of the chamber read by the CCD's which is shown expanded on the right, where the observed pulse shape is exhibited. The peak values have been plotted on the layout at the left.

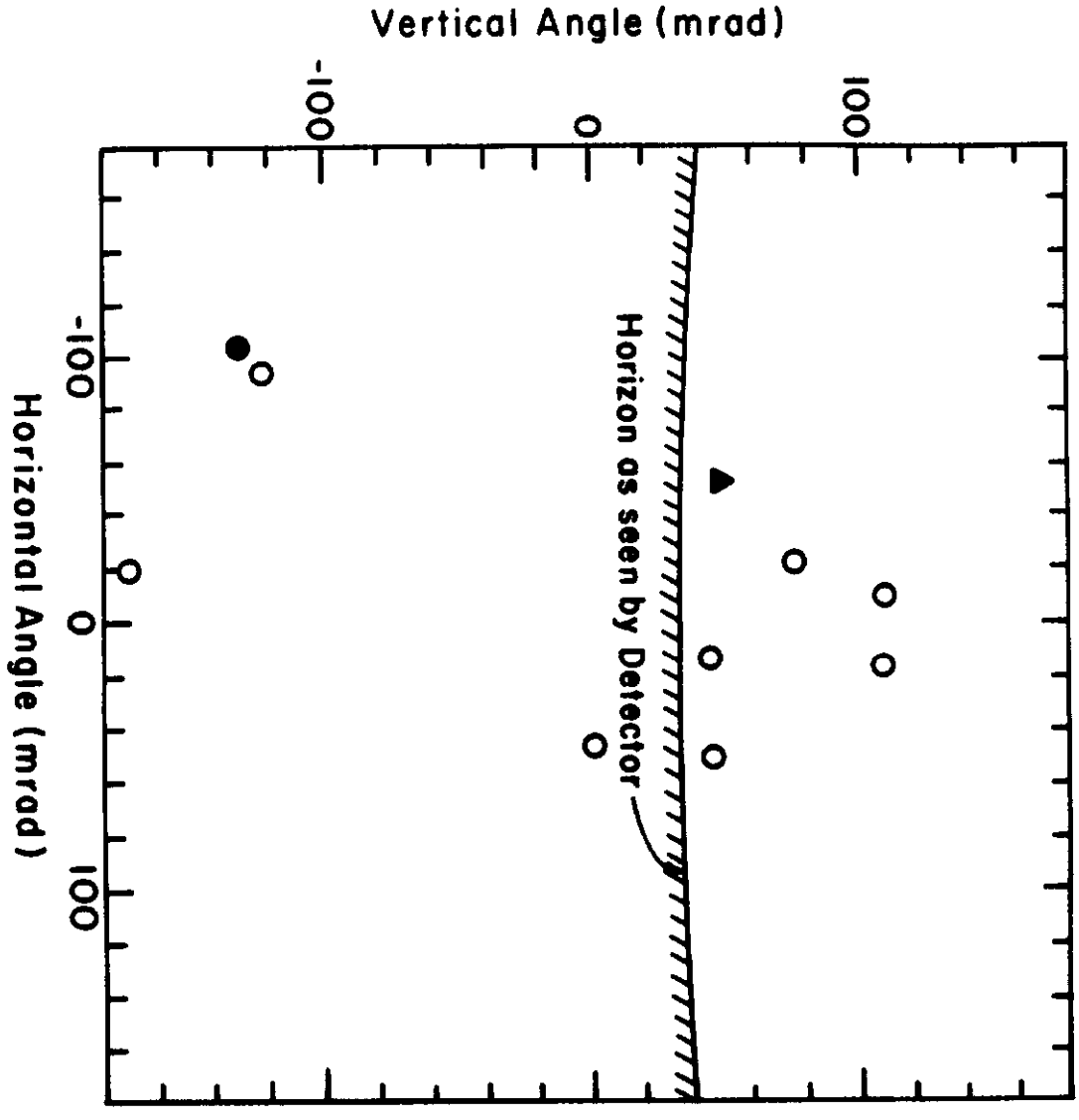

FIGURE 9

Scatter plot of the angular distribution of candidate events. Only the bold-faced point has energy >3 GeV; the triangular point has energy >2 GeV, but unambiguously does not point toward the dump. The three points apparently emergent from below the horizon are actually cosmic rays entering the detector from the rear.

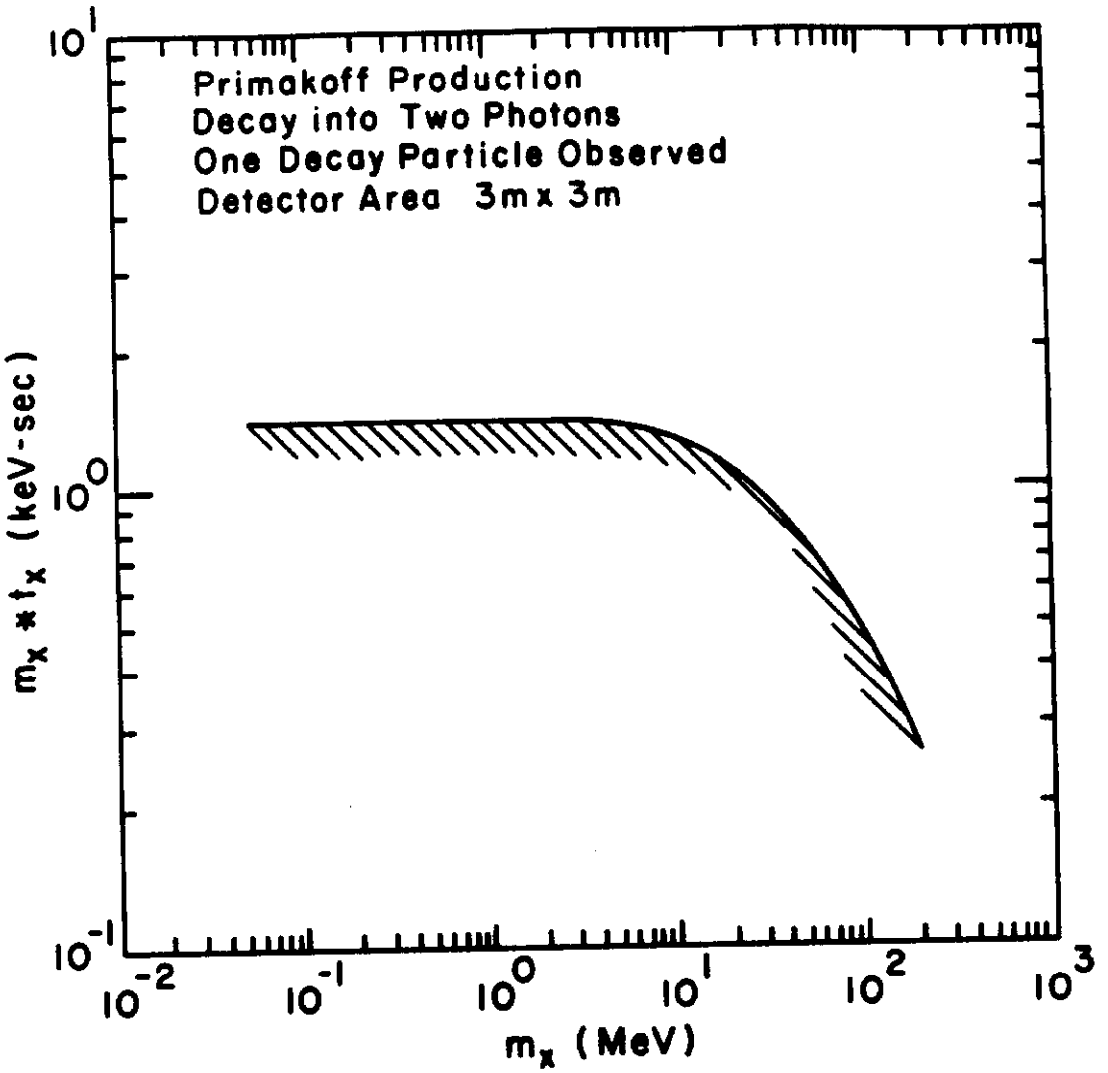

FIGURE 10

Limits (95% confidence level) on hypothetical axion properties from experiment E-137. It is assumed the axion decays predominantly into $\gamma\gamma$.

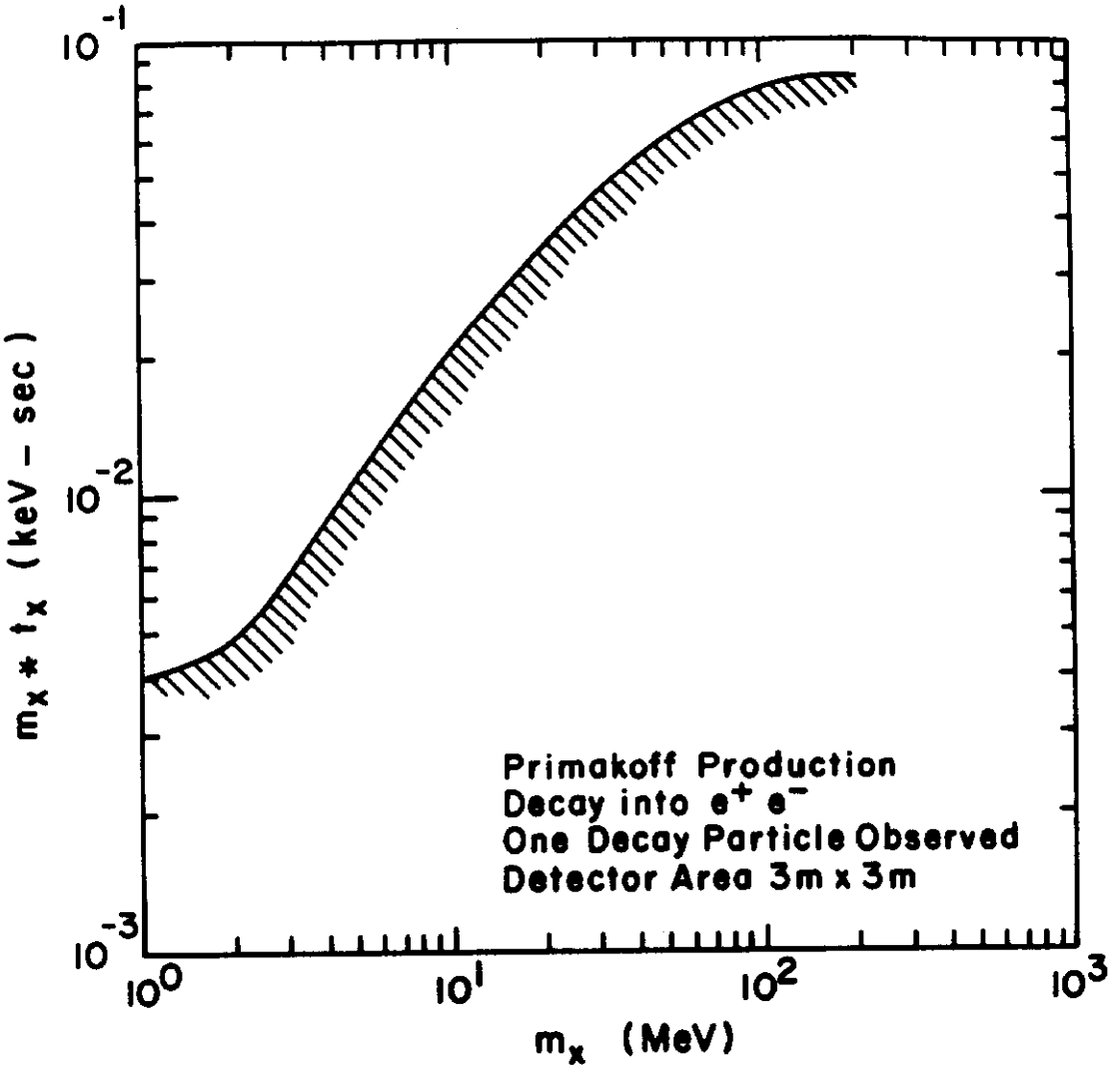

FIGURE 11

Limits on hypothetical axion properties from experiment E-137. It is assumed the axion decays predominantly into $e^+ e^-$.

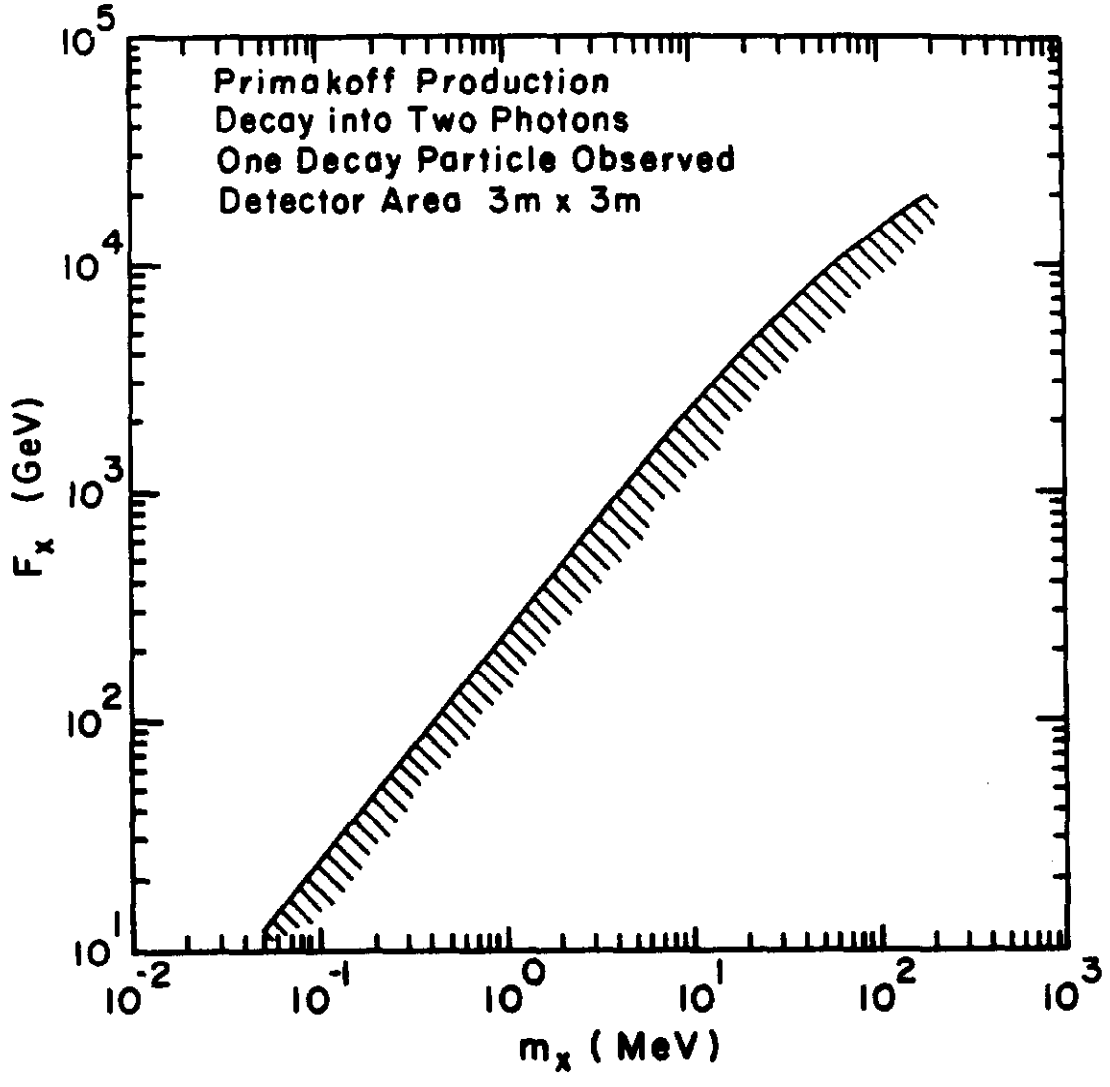

FIGURE 12

Exclusion plot for axion mass and lifetime parameters, assuming Primakoff photoproduction and a standardised "generic" coupling F_x to two photons (cf Appendix I, Eqn. A2).

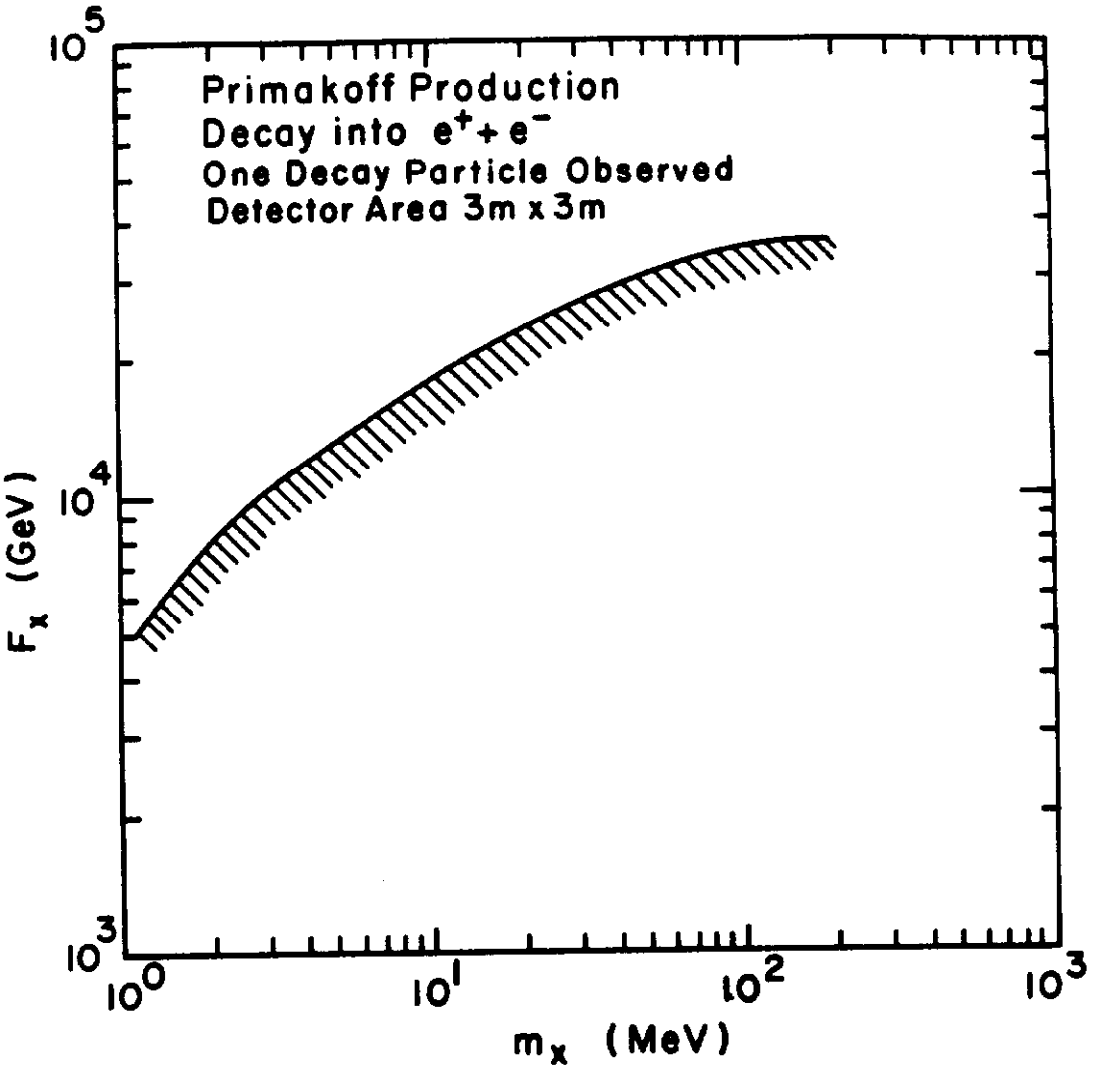

FIGURE 13

Exclusion plot for axion mass and lifetime parameters, assuming Primakoff photoproduction and a standardized "generic" coupling M_x/F_x to electrons (cf Appendix I, Eqn. A3).

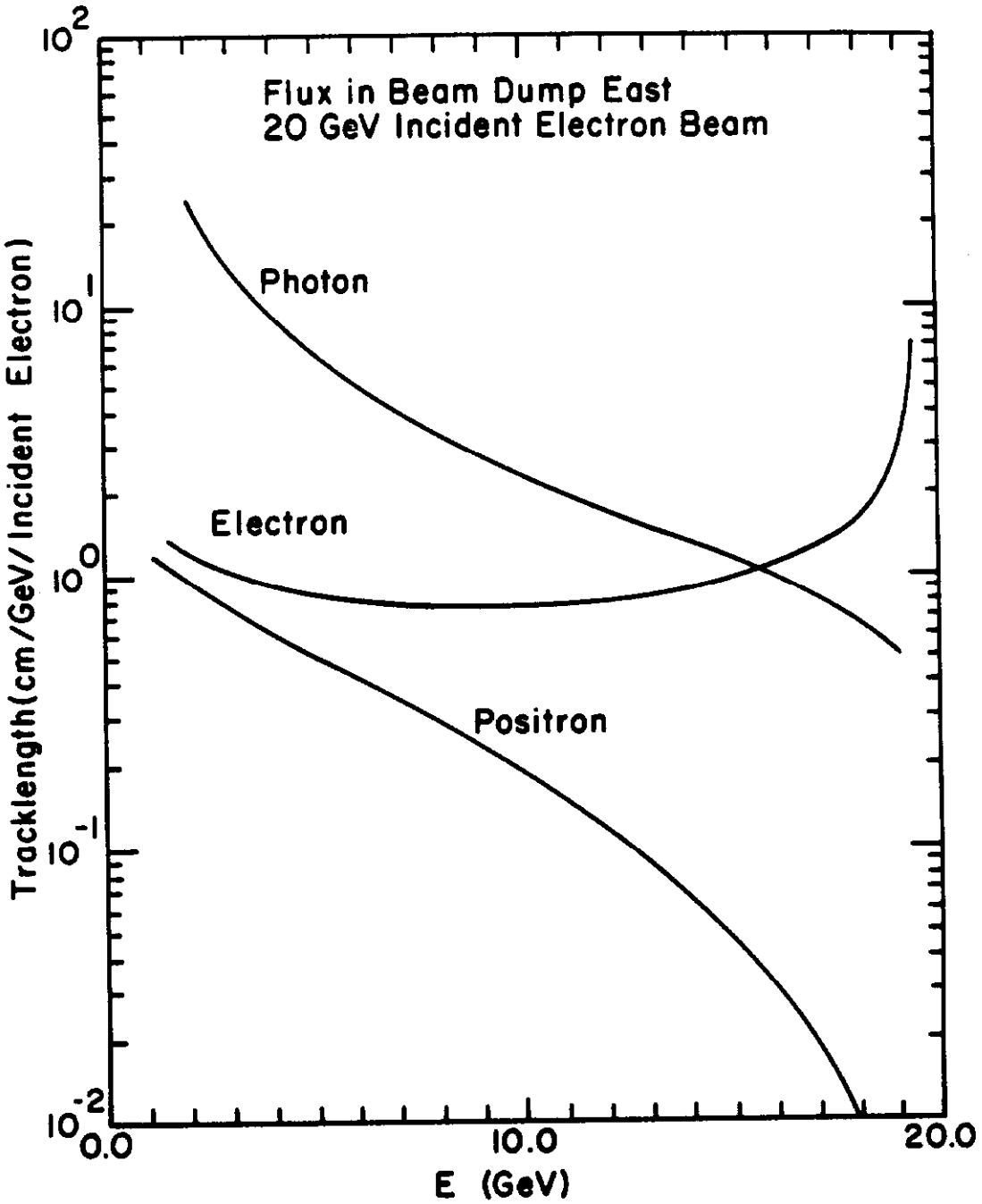

FIGURE 14

Track-length distribution T(E) of photons, electrons and positrons, in the SLAC beam dump. The normalisation is such that, for example the photoproduced axion yield dN/dE per incident is given by

$$\frac{dN}{dE} = T(E) \cdot \sum_Z \sigma(\gamma+Z \to x+Z) P_Z$$

where P_Z is the number density of atoms (per cm^{-3}) of atomic number Z.

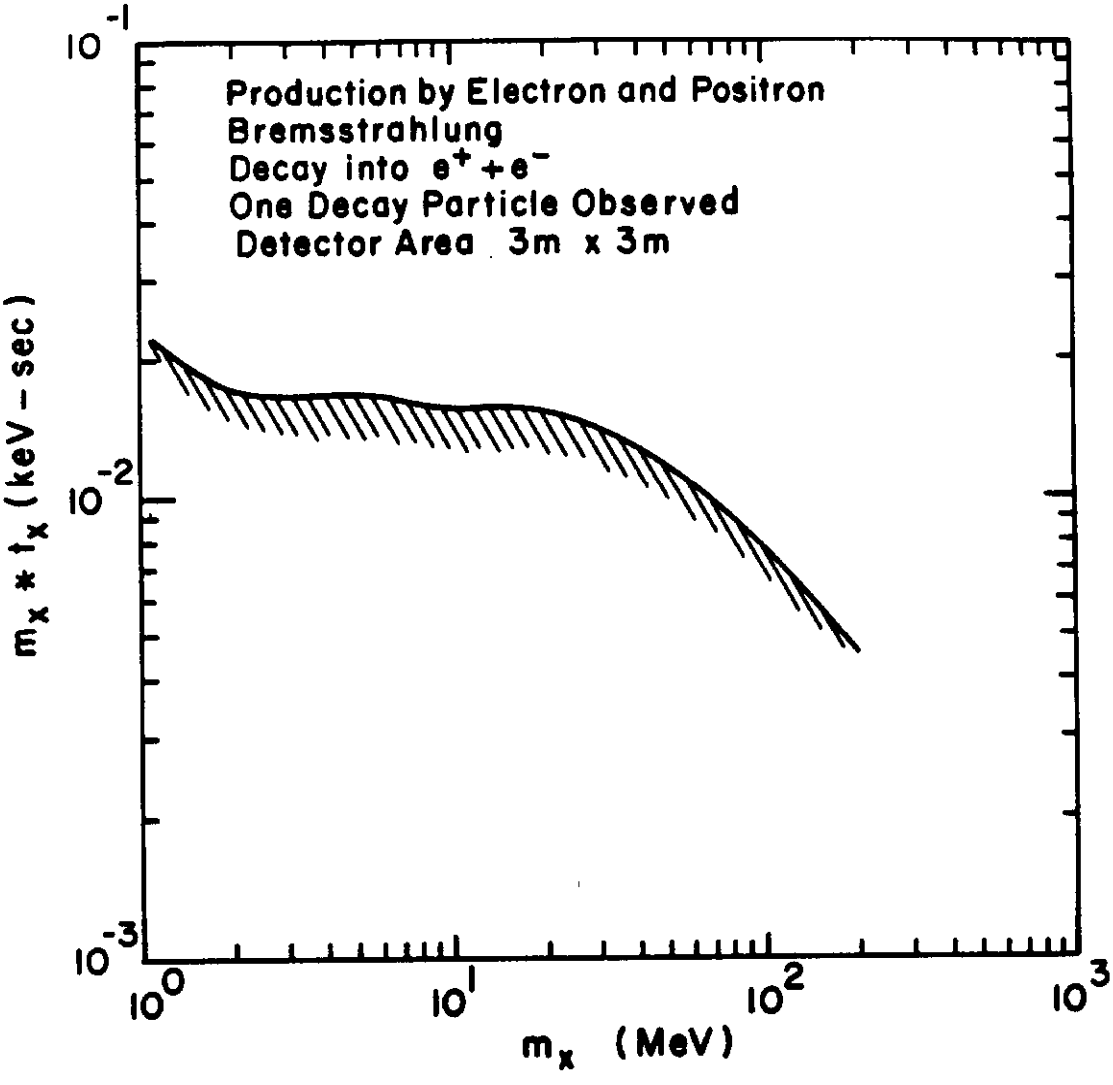

FIGURE 15

Exclusion plot for axion mass and lifetime parameters assuming bremsstrahlung from electrons and positrons and a standardised "generic" coupling F_x to $\gamma\gamma$ and e^+e^- (cf Appendix I, Eqns. A2 and A3).

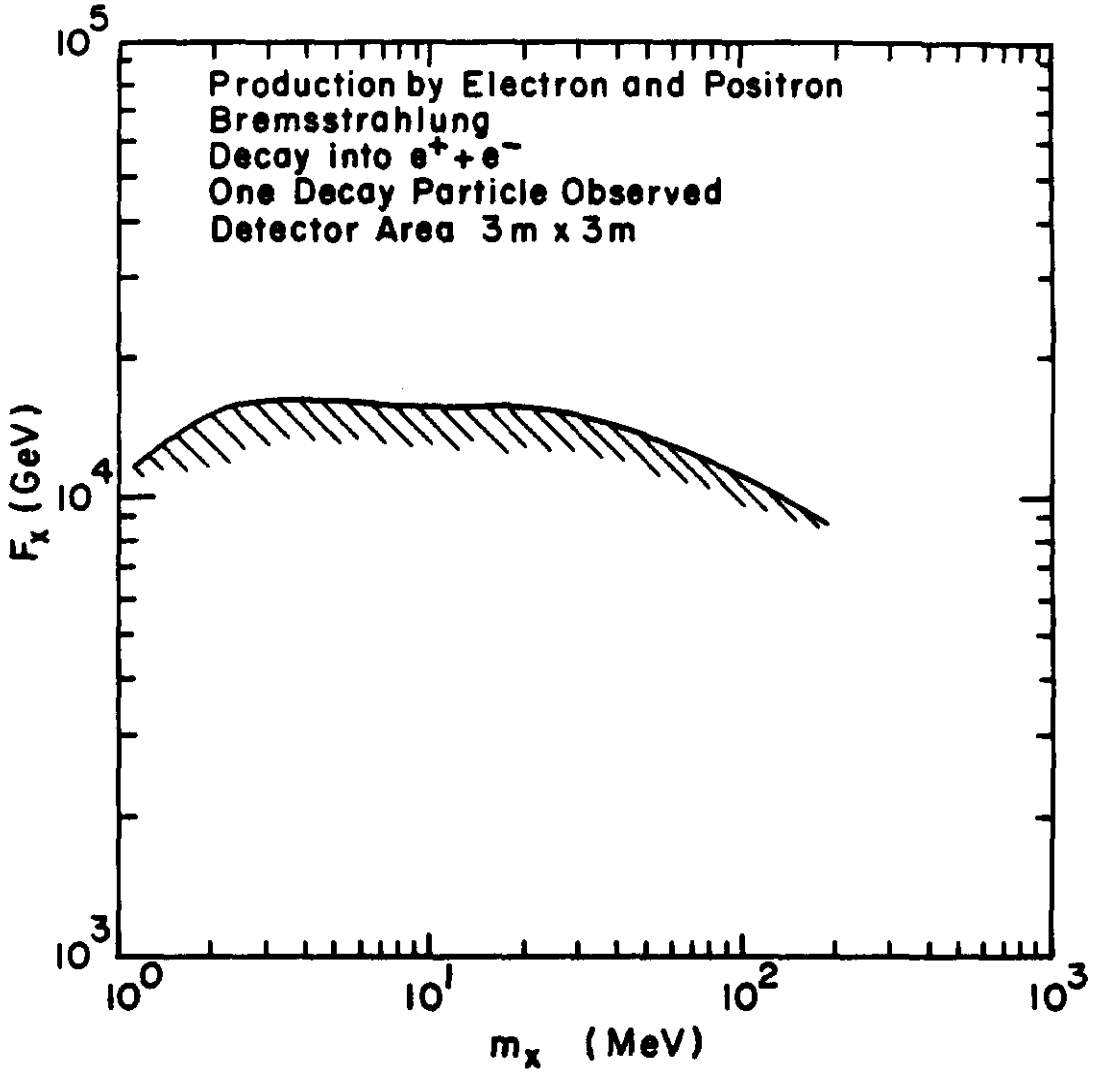

FIGURE 16

Exclusion plot as in Fig. 15 for F_x and m_x.

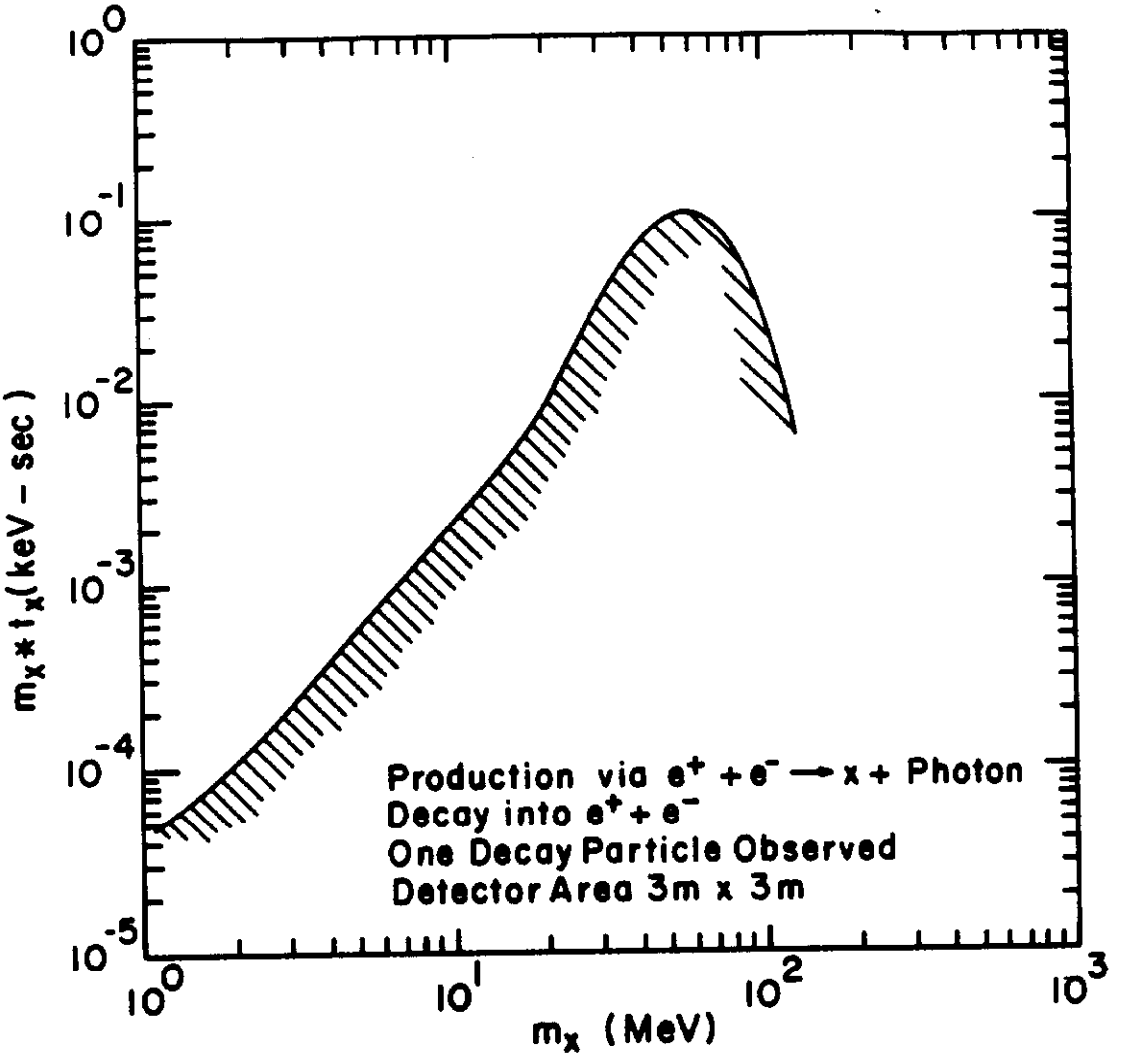

FIGURE 17

Exclusion plot for axion mass and lifetime parameters assuming positron annihilation on atomic electrons via $e^+e^- \rightarrow x + \gamma$ and subsequent decay into e^+e^-.

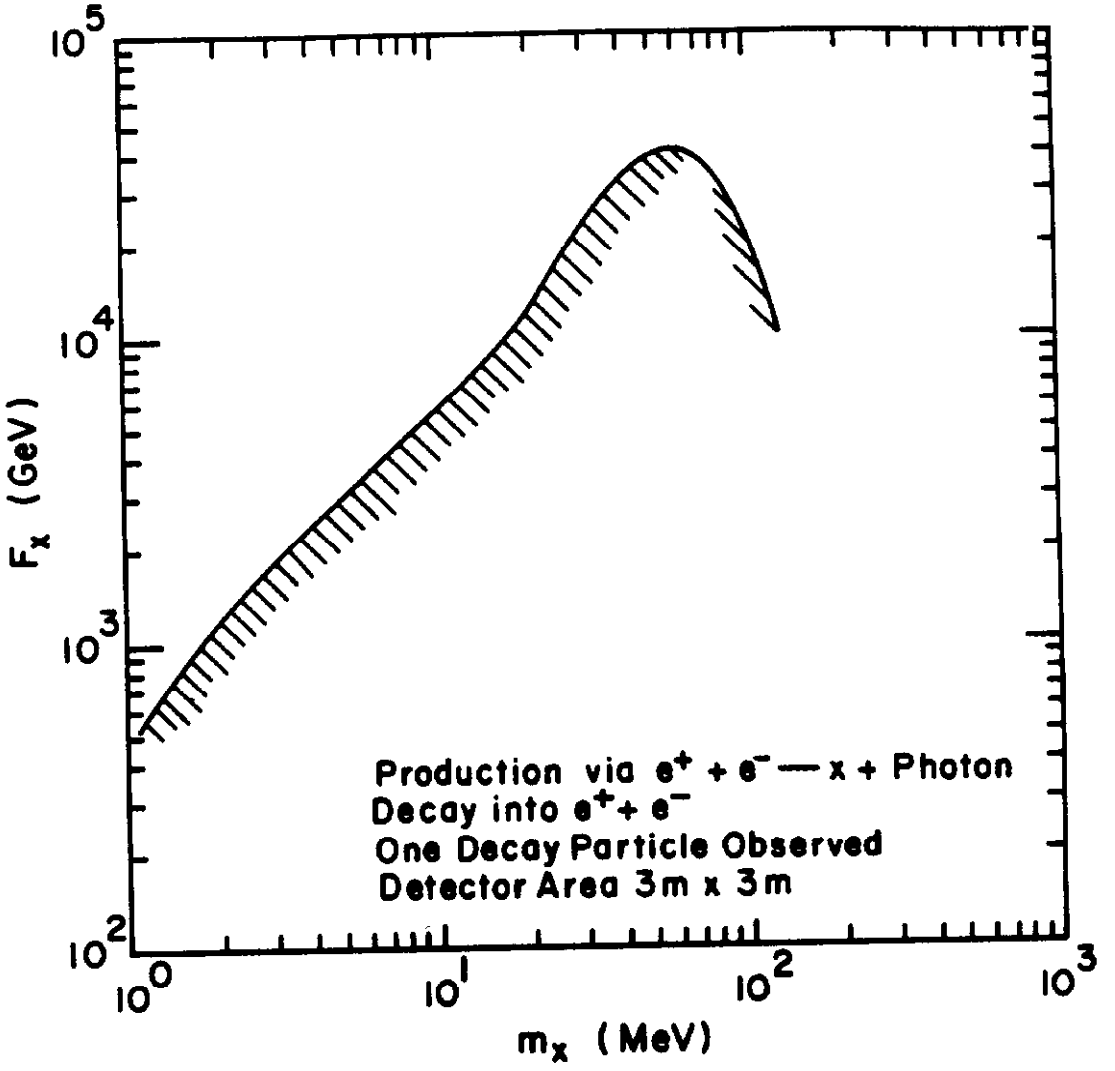

FIGURE 18

Exclusion plot as in Fig. 17 for F_x and m_x.

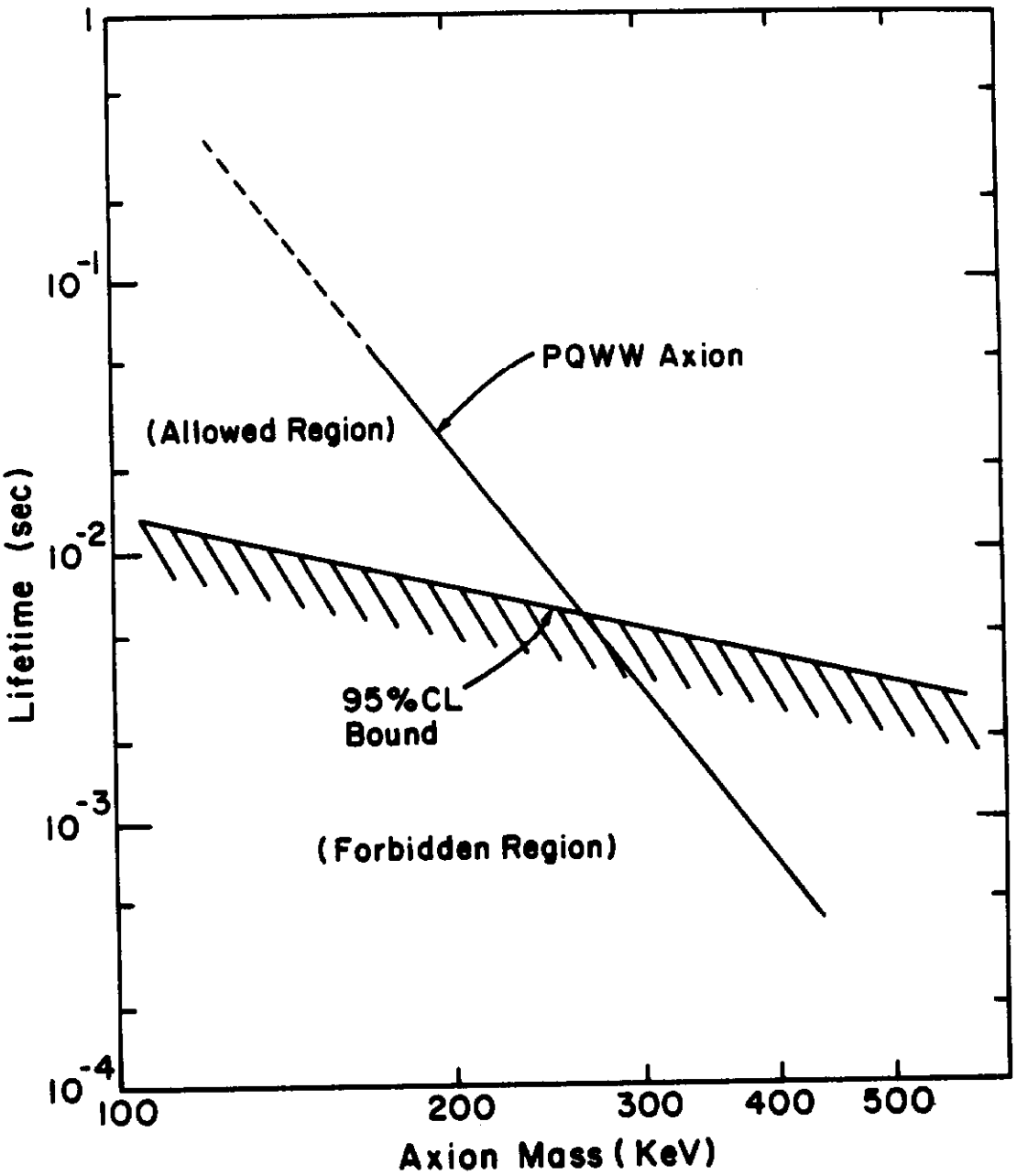

FIGURE 19

Limits on axion properties assuming coupling only to $\gamma\gamma$; the predicted properties of the PQWW axion are also shown.

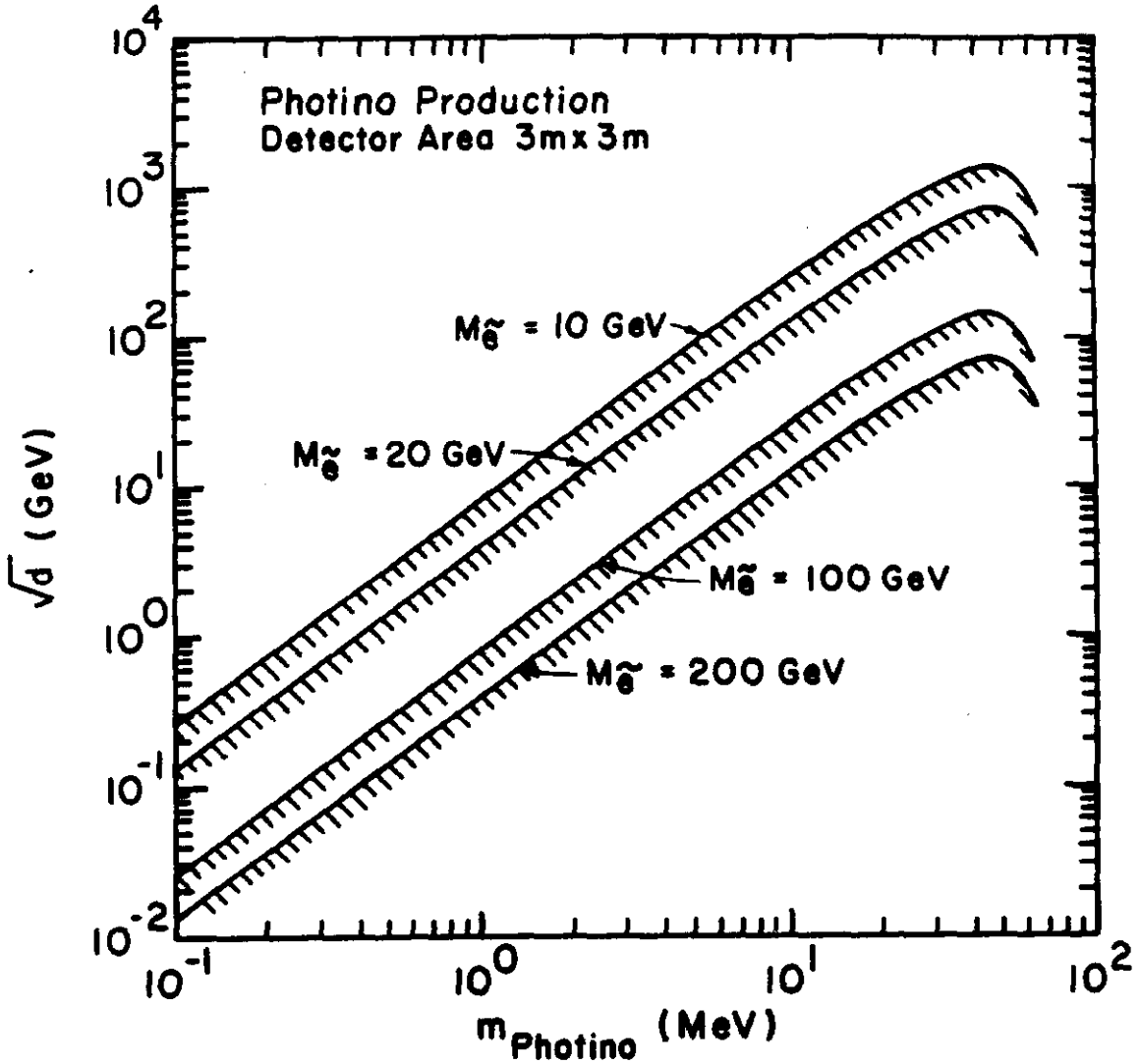

FIGURE 20

Exclusion plot for photino mass as function of symmetry breaking scale $\sqrt{d}$ and assumed selectron mass, as discussed in the text and Appendix A.